Article

Substituent-Guided Cluster Nuclearity for Tetranuclear Iron(III) Compounds with Flat {Fe$_4$(μ$_3$-O)$_2$} Butterfly Core

Lorenzo Marchi [1], Stefano Carlino [2], Carlo Castellano [2], Francesco Demartin [2], Alessandra Forni [3], Anna M. Ferretti [4], Alessandro Ponti [4], Alessandro Pasini [2] and Luca Rigamonti [1,2,*]

[1]   Dipartimento di Scienze Chimiche e Geologiche, Università degli Studi di Modena e Reggio Emilia, Via G. Campi 103, 41125 Modena, Italy; lorenzo.marchi@unimore.it
[2]   Dipartimento di Chimica, Università degli Studi di Milano, Via C. Golgi 19, 20133 Milano, Italy; stefano04.85@gmail.com (S.C.); carlo.castellano@unimi.it (C.C.); francesco.demartin@unimi.it (F.D.); alessandro.pasini@unimi.it (A.P.)
[3]   Istituto di Scienze e Tecnologie Chimiche "Giulio Natta", Consiglio Nazionale delle Ricerche (SCITEC-CNR), Via C. Golgi 19, 20133 Milano, Italy; alessandra.forni@scitec.cnr.it
[4]   Istituto di Scienze e Tecnologie Chimiche "Giulio Natta", Consiglio Nazionale delle Ricerche (SCITEC-CNR), Via G. Fantoli 16/15, 20138 Milano, Italy; anna.ferretti@scitec.cnr.it (A.M.F.); alessandro.ponti@scitec.cnr.it (A.P.)
*   Correspondence: luca.rigamonti@unimore.it; Tel.: +39-059-205-8646

Abstract: The tetranuclear iron(III) compounds [Fe$_4$(μ$_3$-O)$_2$(μ-L^Z)$_4$] (**1–3**) were obtained by reaction of FeCl$_3$ with the shortened salen-type N$_2$O$_2$ tetradentate Schiff bases *N*,*N'*-*bis*(salicylidene)-*o*-Z-phenylmethanediamine H$_2$L^Z (Z = NO$_2$, Cl and OMe, respectively), where the one-carbon bridge between the two iminic nitrogen donor atoms guide preferentially to the formation of oligonuclear species, and the *ortho* position of the substituent Z on the central phenyl ring selectively drives towards Fe$_4$ bis-oxido clusters. All compounds show a flat almost-symmetric butterfly-like conformation of the {Fe$_4$(μ$_3$-O)$_2$} core, surrounded by the four Schiff base ligands, as depicted by both the X-ray molecular structures of **1** and **2** and the optimized geometries of all derivatives as obtained by UM06/6-311G(d) DFT calculations. The strength of the antiferromagnetic exchange coupling constants between the iron(III) ions varies among the three derivatives, despite their magnetic cores remain structurally almost unvaried, as well as the coordination of the metal ions, with a distorted octahedral environment for the two-body iron ions, Fe$_b$, and a pentacoordination with trigonal bipyramidal geometry for the two-wing iron ions, Fe$_w$. The different magnetic behavior within the series of examined compounds may be ascribed to the influence of the electronic features of Z on the electron density distribution (EDD) of the central {Fe$_4$(μ$_3$-O)$_2$} core, substantiated by a Quantum Theory of Atoms In Molecules (QTAIM) topological analysis of the EDD, as obtained by UM06 calculations **1–3**.

Keywords: tetradentate ligands; Schiff bases; oligonuclear complexes; X-ray structures; magnetic properties; DFT calculations; halogen bond

1. Introduction

The need for miniaturized devices for technological applications is driving scientific research into the replacing of existing materials with molecular species of nanometer sizes [1–4]. Polynuclear compounds of transition metal ions are very promising materials for this purpose because of their tunable electronic and magnetic properties [5–8], achieved through the modulation of the magnetic exchange interactions. In the search for this variability, until a few years ago, the serendipitous assembly approach led to a huge increase in the amount of synthesized polynuclear complexes with different bridging ligands [9], but a rational approach is most desirable, with precise control of the obtained compounds and their properties by the modification of the ligands [10] and the synthetic conditions [11–13].

Schiff bases are well-known ligands that have been used for decades in the synthesis of metal complexes for applications in different fields, such as catalysis [14], new materials and optics [15–17]. From the most famous N_2O_2 tetradentate Schiff base H_2salen, formed by the condensation of salicylaldehyde (salH) with ethylenediamine (en) [18–20], new functionalized families of structurally modified molecules have been designed for the purpose of obtaining new polynuclear complexes with desired structural features and functionalities [21–23]. In particular, the substitution of en with the shorter methylenediamine in condensation with salH yields ligands (called H_2salben's when the methylene bridge between the two nitrogen atoms carries a phenyl ring) that preferentially produce oligonuclear compounds by complexation [24–27].

Based on our previous experience in working with Schiff bases and the preferred isolation of oligonuclear metal clusters [8,24–31], in this work, we decided to exploit the metal complexation ability toward iron(III) of three H_2sal(*o*-Z)ben derivatives bearing a substituent Z in the *ortho* position of the central phenyl ring (*N,N'*-*bis*(salicylidene)-*o*-Z-phenylmethanediamine) [24,32] (abbreviated as H_2L^Z in this paper) with Z going from NO_2 to Cl and OMe (Scheme 1). The tetranuclear iron(III) compounds $[Fe_4(\mu_3\text{-}O)_2(\mu\text{-}L^Z)_4]$ (**1–3**, with Z = NO_2, Cl, OMe, respectively, see Scheme 1) could be selectively obtained by reaction with $FeCl_3$ in contrast with the formation of dinuclear species $[Fe_2((\mu\text{-}OMe)_2(\mu\text{-}sal(p\text{-}Y)ben)_2]$ when ligands with substituents Y in *para* position or absent were employed [27]. Here, we report the synthesis and the structural and magnetic characterization of these complexes, revealing the modulation of Z on the exchange coupling constants between the iron ions within the three derivatives. The topological analysis of the computed electron density distribution (EDD) of **1–3** will help to discuss the electronic effect of Z.
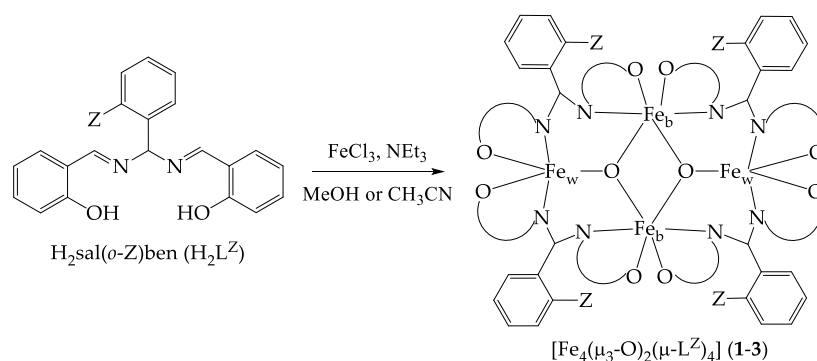
Scheme 1. Synthetic scheme of **1–3** (Z = NO_2, Cl, OMe, respectively) and drawing of the arrangement of the Schiff base ligands around the $\{Fe_4(\mu_3\text{-}O)_2\}$ butterfly core (sal moieties are sketched as ∩ for clarity; iron ions are divided into those of two body, Fe_b, and two wing, Fe_w, ions, as applicable in butterfly-like Fe_4 clusters).

2. Results and Discussion

2.1. Synthesis and X-ray Crystal Structures

The reaction of H_2L^Z with $FeCl_3$ in non-anhydrous MeOH or MeCN in the presence of NEt_3 as a base gave the tetranuclear complexes **1–3** good yields (see Scheme 1), with the best ones in MeOH. The polynucleation ability of the salben ligands due to the one-carbon bridge between the two iminic nitrogen atoms is clearly confirmed here [24–27]. There is also the control on the nature of the oligonuclear compound upon substituent shift, since the dinuclear species $[Fe_2((\mu\text{-}OMe)_2(\mu\text{-}sal(p\text{-}Y)ben)_2]$ are isolated when ligands with substituents Y in *para* position or absent were employed [27]. The tetranuclear nature of **1–3** is proven by the ESI^+ mass spectra with the $[M+Na]^+$ and $[M+1]^+$ peaks and the fragmentation of the $[Fe_3(O)(L^Z)_3]^+$ ions (see Experimental Section). Furthermore, single crystals suitable for the X-ray structure determination of **1**·1.5*i*Pr_2O and **2**·2*i*Pr_2O were obtained, and the crystal structures could be refined.

The asymmetric unit of **1**·1.5*i*Pr_2O contains two independent clusters $[Fe_4(\mu_3\text{-}O)_2(\mu\text{-}L^{NO2})_4]$, A and B, structurally very similar (see Figure S1 for molecule A and an overlap

of A and B in Figure S2a in Supplementary Materials), and three *i*Pr$_2$O solvent molecules, clathrated in the lattice voids. For **2·2*i*Pr$_2$O**, in contrast, only one independent molecule of [Fe$_4$(μ$_3$-O)$_2$(μ-L^{Cl})$_4$] and two *i*Pr$_2$O molecules are present in the asymmetric unit (Figure 1). Both molecules of **1** and **2** show four iron(III) ions linked together by two triply-bridging oxido anions, giving the {Fe$_4$(μ$_3$-O)$_2$} core. The four dianionic tetradentate ligands sal(*o*-Z)ben$^{2−}$ surround the core, bridging two iron ions each, as shown in Scheme 1 and Figure 1 and Figure S1 in Supplementary Materials.


(a) **(b)**
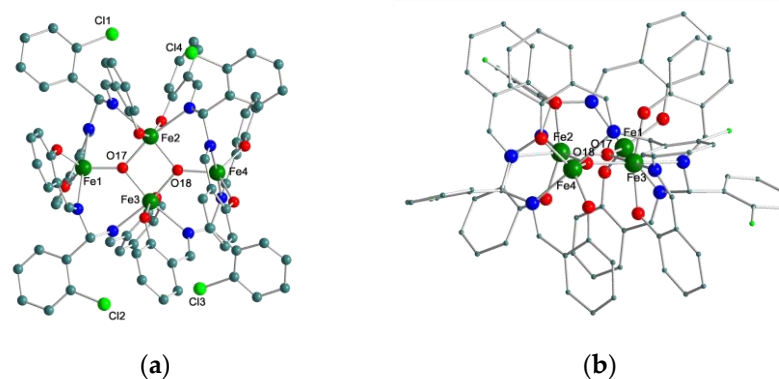
Figure 1. (**a**) Molecular structure of [Fe$_4$(μ$_3$-O)$_2$(μ-L^{Cl})$_4$] (**2**) (Fe = dark green, O = red, N = blue, Cl = light green, C = grey; hydrogen atoms omitted for clarity). Fe1 and Fe4 are the Fe$_w$ ions, while Fe2 and Fe3 are the Fe$_b$ ions. (**b**) View of the tetranuclear cluster **2** almost along the Fe$_4$O$_2$ plane, highlighting the flat core.

In such clusters, the {Fe$_4$(μ$_3$-O)$_2$} core adopts a so-called butterfly-like conformation where the iron(III) ions are usually divided into two 'body', Fe$_b$ (Fe2, Fe3), and two 'wing', Fe$_w$ (Fe1, Fe4), metal ions [33]. In this butterfly-like conformation, the Fe2–Fe3 fragment features the body of the butterfly, and the Fe1Fe2Fe3 and Fe2Fe3Fe4 triangles schematize the wings, with the Fe1 and Fe4 occupying the tip positions. The Fe$_4$O$_2$ moieties are essentially planar, with maximum displacements from the least square (l.s.) planes of only 0.082 (Fe4A) and 0.064 Å (Fe4B) for **1**, and 0.027 Å (O17) for **2** (see Figure 1 and Figure S1 in Supplementary Materials). Another proof of the planarity of the metal cores can be detected through the dihedral angles between the l.s. planes defined by the two wings, which are 176.9 and 176.2° (molecules A and B, respectively) in **1** and 179.1° in **2**, very close to the ideal value of 180°. There are few other cases that have been reported in which the two wings lie in the same plane [34–37], but they are usually associated with higher displacement values of the oxido ions from the Fe$_3$ planes, which is not the case here.

The μ$_3$-O bridges in **1** are asymmetric: the Fe$_w$–O distances (average 1.790 Å) are shorter than the Fe$_b$–O ones (average 1.960 Å). Similar asymmetry is also present in **2,** with a short Fe$_w$–O average distance of 1.802 Å and a long Fe$_b$–O average distance of 1.945 Å (see Table S1 in Supplementary Materials). This feature is in line with values reported in the literature for butterfly-like Fe$_4$O$_2$ clusters [33], in which the Fe$_w$–O distances of our compounds are among the shortest observed. The μ$_3$-O bridge asymmetry is evident also by analyzing the Fe–O–Fe angles, ranging from 130.0(3)° to 133.2(3)° in **1** and from 127.81(6)° to 132.71(6)° in **2** for Fe$_w$–O–Fe$_b$, while the values are much smaller for Fe$_b$–O–Fe$_b$ (from 96.7(2)° to 97.2(2)° in **1** and 99.31(5)° and 99.64(6)° in **2** (see Table S1 in Supplementary Materials for all values). The opening of the Fe$_b$–O–Fe$_b$ angles in **2** leads to a slightly longer Fe$_b$···Fe$_b$ distance (2.9683(4) Å) compared to **1** (2.929(2) and 2.937(2) Å) and to an asymmetry in the Fe$_w$ position that brings Fe1 and Fe4 closer to Fe3, compared to Fe2 in **2** (Fe1···Fe2 = 3.4241(4) Å, Fe1···Fe3 = 3.3738(5) Å, and Fe4···Fe2 = 3.4211(5) Å, Fe4···Fe3 = 3.3737(4) Å), while all the Fe$_w$···Fe$_b$ distances range around 3.41 Å in **1**.

Considering the metal coordination, the two Fe$_w$ ions have a trigonal bipyramidal (*tb*) coordination (see Figure 1 and Figure S1 in Supplementary Materials), while usually they show an octahedral (*oh*) geometry [33–51]; this feature can be ascribed to the 'strain'

induced by the Schiff base ligands. Considering the trigonal plane formed by the three oxygen atoms coordinated to Fe_w, the *tb* polyhedra are rotated on average by 70° (**1**) and 84° (**2**) with respect to each other and by about 55° (**1**) and 48° (**2**) with respect to the Fe_4O_2 l.s. plane. The two Fe_b ions have instead quite a distorted octahedral coordination, still due to the 'strained' surrounding ligands (see Table S1 in Supplementary Materials).

The asymmetry in the wing iron ion positions and the different rotation of the *tb* polyhedra can probably be explained by crystal packing and/or the steric and electronic effects of the Z substituents. In particular, the arrangement of the four sal(*o*-Cl)ben^{2-} ligands around the $\{Fe_4(\mu_3\text{-}O)_2\}$ core in **2** is noteworthy, where each of the chlorine atoms points towards the center of the adjacent phenyl ring, giving rise to a C–Cl···π halogen bond [52] (average distance of Cl from the l.s. plane through the phenyl ring = 3.66 Å, see Figure 1), due to the interaction between the positive region of the electrostatic potential on the halogen along the extension of the C–Cl bond with the π system of the phenyl ring [53–55]. On the other hand, the nitro group in **1** is unable to produce a stabilizing interaction with the π system of the adjacent phenyl ring, determining a more irregular arrangement of the four sal(o-NO$_2$)ben^{2-} ligands with respect to the $\{Fe_4(\mu_3\text{-}O)_2\}$ core (see Figure S1 in Supplementary Materials). This feature also leads to slightly different conformations of the surrounding ligands, mainly affecting the central phenyl ring carrying the substituent Z, as is clearly perceivable by superimposing the two structures (see Figure S2b in Supplementary Materials for the overlap of **1**A and **2**).

The Fe–O bonds involving the phenoxido oxygen atoms of the Schiff base ligands are in the range 1.865(5)–1.964(5) Å for **1** and 1.8660(12)–1.9698(13) Å for **2**, with usually shorter distances when the wing Fe1 and Fe4 ions are involved. Fe–N bonds are longer than Fe–O ones, ranging from 2.160(6) to 2.234(6) Å in **1** and from 2.1509(15) to 2.2730(13) Å in **2**, but they show the same trend with respect to Fe_w and Fe_b. It is instead hard to discern a direct effect of the substituent Z on the coordination distances.

2.2. Optimized Geometries

Aimed at confirming the stability of **3** and ascertaining the influence of Z, if any, on the coordination distances of the iron ions, UM06/6-311G(d) calculations were performed on **1–3**. Selected distances are reported in Table 1 in direct comparison with the corresponding experimental ones. The resulting optimized structures are essentially symmetric, unlike the experimental ones, which show a slight degree of asymmetry as described above, probably due to crystal packing effects. The comparison of the Fe_w–O and Fe_b–O computed distances with the corresponding experimental average values in **1** and **2** indicates an overall good agreement, with just a little overestimate for the former (1.818 and 1.825 Å vs. 1.790(5) and 1.802(11) Å, respectively) and a better correspondence for the latter (1.951 and 1.947 Å vs. 1.960(5) and 1.945(11) Å, respectively (see Figure S2c,d in Supplementary Materials for an overlap of the optimized and experimental structures).

The computed structures evidence a minor influence of the Z groups on the coordination bond lengths of the central $\{Fe_4(\mu_3\text{-}O)_2\}$ cores by comparing the corresponding bond lengths in **1**, **2** and **3**, with the Fe_w–O and Fe_b–O distances slightly increasing (1.818, 1.825, 1.829 Å) and decreasing (1.951, 1.947, 1.944 Å), respectively, going from Z = NO$_2$ to Cl and then to OMe. The remaining Fe–O distances do not show significant variations along the same series (Fe_w–O is essentially unvaried, Fe_b–O slightly increases from 1.956 to 1.960 and 1.967 Å), while more significant, though still small, variations are observed in the Fe–N distances, which decrease for both Fe_w (2.170, 2.157, 2.150 Å) and Fe_b (2.225, 2.224, 2.211 Å) ions when going from **1** to **3**. The geometry of the $\{Fe_4(\mu_3\text{-}O)_2\}$ core is only slightly different in the three complexes, with a lengthening of the Fe_w···Fe_w distance up to 0.028 Å and shortening of the Fe_b···Fe_b one equal to 0.023 Å going from the electron-withdrawing NO$_2$ group to the electron-donating OMe group. As already evidenced in previous studies on copper(II) complexes of salen analogues with push–pull structures [15], NO$_2$ exerts the strongest electronic effect on the coordination geometry with respect to OMe.

Table 1. Selected experimental (first row, if available) and UM06/6-311G(d) computed (second row, figures in italics) distances (Å) for **1**, **2** and **3** [1,2].

	1·1.5*i*Pr₂O [3]	**2·2*i*Pr₂O**	**3**
Fe1–O17	1.784(5), 1.783(5)	1.7994(11)	–
	1.818	*1.825*	*1.829*
Fe4–O18	1.797(5), 1.789(5)	1.8040(11)	–
	1.818	*1.825*	*1.829*
Fe2–O17	1.948(5), 1.979(5)	1.9380(12)	–
	1.951	*1.947*	*1.944*
Fe2–O18	1.967(5), 1.964(5)	1.9461(11)	–
	1.951	*1.946*	*1.944*
Fe3–O17	1.970(5), 1.948(5)	1.9567(11)	–
	1.951	*1.946*	*1.944*
Fe3–O18	1.939(5), 1.967(5)	1.9389(12)	–
	1.951	*1.947*	*1.944*
Fe1–O1	1.865(5), 1.865(5)	1.9021(13)	–
	1.892	*1.891*	*1.891*
Fe1–O5	1.925(5), 1.925(5)	1.8662(12)	–
	1.892	*1.889*	*1.891*
Fe1–N1	2.160(6), 2.165(7)	2.1636(11)	–
	2.170	*2.158*	*2.150*
Fe1–N4	2.193(6), 2.171(6)	2.1930(15)	–
	2.170	*2.157*	*2.150*
Fe2–O4	1.964(5), 1.924(5)	1.9698(13)	–
	1.956	*1.960*	*1.967*
Fe2–O13	1.954(5), 1.915(6)	1.9319(11)	–
	1.956	*1.959*	*1.967*
Fe2–N3	2.211(6), 2.198(7)	2.2609(12)	–
	2.225	*2.224*	*2.211*
Fe2–N10	2.207(7), 2.233(6)	2.2729(13)	–
	2.224	*2.224*	*2.211*
Fe1···Fe2	3.426(2), 3.427(2)	3.4241(4)	–
	3.419	*3.424*	*3.427*
Fe1···Fe3	3.402(2), 3.406(2)	3.3738(5)	–
	3.419	*3.426*	*3.427*
Fe4···Fe2	3.413(2), 3.415(2)	3.4210(5)	–
	3.419	*3.426*	*3.427*
Fe4···Fe3	3.420(2), 3.428(2)	3.3736(4)	–
	3.419	*3.424*	*3.427*
Fe1···Fe4	6.168(2), 6.172(2)	6.1128(7)	–
	6.155	*6.174*	*6.183*
Fe2···Fe3	2.929(2), 2.937(2)	2.9683(4)	–
	2.980	*2.965*	*2.957*

[1] O17 and O18 are the triply bridging oxido ions; [2] Fe1 and Fe4 are Fe$_w$, while Fe2 and Fe3 are Fe$_b$; [3] the double experimental values are referred to molecules A and B, respectively.

It is worth noting that the calculations correctly reproduce the Cl···π interaction observed in the crystal structure, providing Cl distances from the ring centroids equal to 3.668 and 3.660 Å. This agreement can be ascribed to the ability of the M06 functional to describe weak dispersion-dominated interactions, unlike the B3LYP functional, which has been shown to be unable to model the C–X···π halogen bond [53–55]. According to previous CCSD(T) calculations at the complete basis set limit on model systems constituted by benzene and DCl dimers (D = H, HCC, F and NC) in a T-shaped configuration [54], the energy associated with this interaction ranges from –1.43 to –3.38 kcal mol^{-1} at the respective equilibrium distances (from 3.45 to 3.25 Å), according to the electron-withdrawing ability of the D group. It is then expected that the C–Cl···π interaction in **2**, while present, is however quite weak, owing to the observed large Cl···π distance and the non-optimal T-shaped arrangement of the interacting species.

By analyzing the conformation of the ligands in the optimized geometries of **1–3** (see Figure S2e in Supplementary Materials), it is apparent the different orientation of the central phenyl ring carries the substituent Z, similar to the experimental structures, while the cores and the coordination environments of the four iron ions are almost superimposed. Moreover, the computed reciprocal rotations of the two *tb* polyhedra with respect to each other (78.5, 81.1 and 83.5° for **1**, **2** and **3**, respectively) and with respect to the Fe_4O_2 plane (50.8, 49.5 and 48.3° for **1**, **2** and **3**, respectively) show a lower variability with respect to the X-ray crystal structures but follow the same experimental trend. This indicates that, besides crystal packing effects, the intrinsic electronic and steric effects induced by Z are also responsible for the observed conformational differences between **1** and **2** in the solid state.

2.3. Magnetic Properties

The magnetic susceptibility of **1–3** was measured between 5 and 300 K. The product $\chi_M T$ (χ_M is the molar susceptibility referred to an Fe_4 unit) of **1** (Figure 2a) is 16.5 ± 0.3 emu K mol^{-1} Oe^{-1} at 300 K, which is slightly lower than that for four uncoupled iron(III) ions (17.5 emu K mol^{-1} Oe^{-1}, g = 2.00). On cooling, $\chi_M T$ of **1** decreases slowly down to 50 K and more rapidly at lower temperature up until it reaches the value 1.55 ± 0.03 emu K mol^{-1} Oe^{-1} at 5 K. Such behavior suggests that the iron(III) ions are antiferromagnetically coupled and that the coupling is weak.
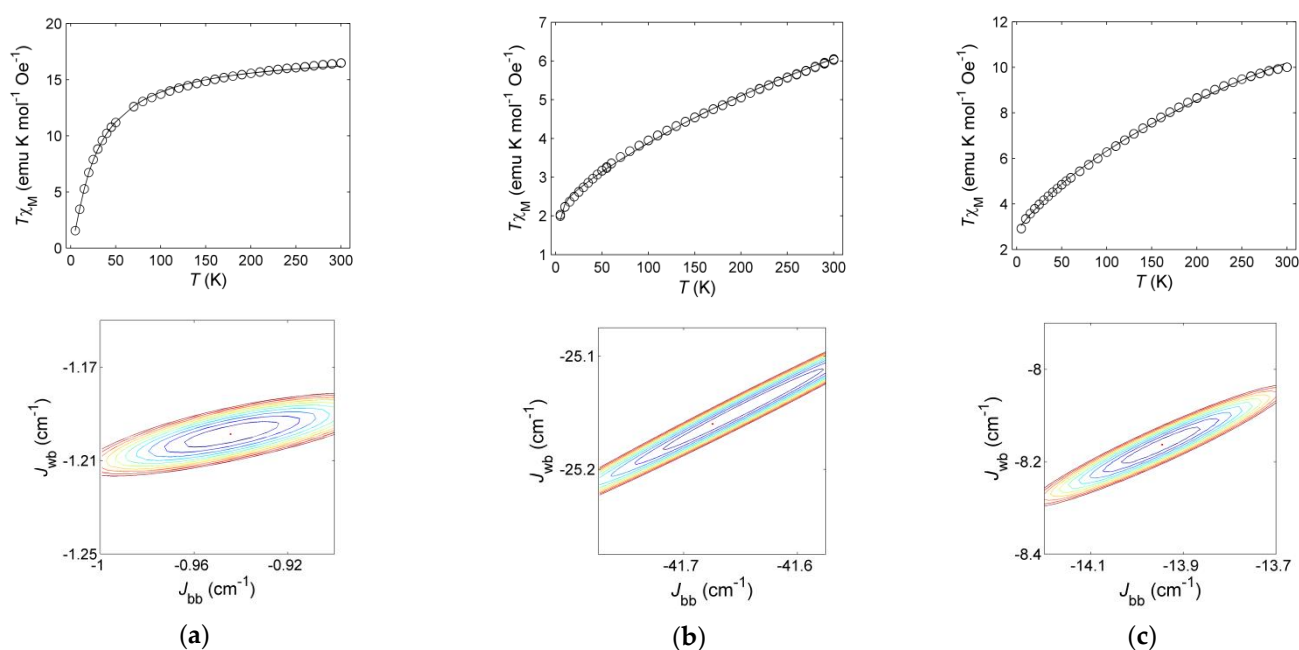

Figure 2. Temperature dependence of the $\chi_M T$ product of (**a**) **1**, (**b**) **2** and (**c**) **3** (χ_M is the molar susceptibility referred to an Fe_4 unit). Top panels: experimental data (circles) and best-fit curves (solid line) based on the simplified butterfly Hamiltonian Equation (1). Bottom panels: constant *ssr* contours from Δ*ssr* = 1 (indigo inner curve) to Δ*ssr* = 10 (brown outer curve); the red dot marks the best-fit point.

The product $\chi_M T$ of **2** and **3** (Figure 2b,c) at 300 K is 6.04 ± 0.02 and 10.0 ± 0.2 emu K mol^{-1} Oe^{-1}, respectively, which is much lower than that of four uncoupled Fe^{3+} ions. For both **2** and **3**, $\chi_M T$ decreases upon cooling but, differently from **1**, the decrease is much less curved between 300 and 5 K. Such results suggest that the antiferromagnetic interactions between the iron ions are stronger in **2** and **3** than in **1**, a conclusion seemingly contrasting with the larger $\chi_M T$ values at low temperature (2.00 ± 0.01 and 2.91 ± 0.06 emu K mol^{-1} Oe^{-1} at 5 K for **2** and **3**, respectively).

Several super-exchange pathways magnetically connect the wing and body iron ions of the planar {$Fe_4(\mu_3\text{-O})_2$} core in **1–3** (see Scheme 2). Thanks to the symmetry of the

cores, all wing–wing super-exchange interactions can be considered equal, and the same assumption can be made for wing–body and body–body interactions. Besides, any magnetic communication through the Schiff base ligands can be neglected because of the longer exchange pathway. Within these approximations, the spin system of **1–3** can be modelled as a butterfly spin system [56] where the exchange couplings are fully determined by the three coupling constants J_{bb} (body–body), J_{wb} (wing–body), and J_{ww} (wing–wing). In complexes **1–3**, the wing–wing exchange can be neglected with respect to the wing–body and body–body interactions because of the longer exchange pathway. By this further assumption, we can set $J_{ww} = 0$ and obtain a simplified butterfly spin system described by the Hamiltonian:

$$\hat{H} = -2J_{bb}\ \hat{\mathbf{S}}_{b1}\cdot\hat{\mathbf{S}}_{b2} - 2J_{wb}\ (\hat{\mathbf{S}}_{w1}\cdot\hat{\mathbf{S}}_{b1} + \hat{\mathbf{S}}_{w1}\cdot\hat{\mathbf{S}}_{b2} + \hat{\mathbf{S}}_{w2}\cdot\hat{\mathbf{S}}_{b1} + \hat{\mathbf{S}}_{w2}\cdot\hat{\mathbf{S}}_{b2}) \tag{1}$$
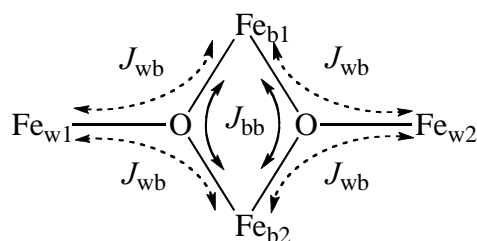
Scheme 2. Magnetic exchange pathways in the simplified butterfly Fe_4 spin system considered during the fitting of the experimental data ($J_{ww} = 0$, see text).

This Hamiltonian can be treated by the Kambe vector coupling method [57], and the energy of the spin states can be expressed as

$$E(|S_{bb}, S_{ww}, S\rangle) = -J_{bb}\ [S_{bb}(S_{bb} + 1) - 35/2] - J_{wb}\ [S(S + 1) - S_{bb}(S_{bb} + 1) - S_{ww}(S_{ww} + 1)] \tag{2}$$

where the spin state $|S_{bb}, S_{ww}, S\rangle$ is labelled as to the two intermediate ($\hat{\mathbf{S}}_{bb} = \hat{\mathbf{S}}_{b1} + \hat{\mathbf{S}}_{b2}$ and $\hat{\mathbf{S}}_{ww} = \hat{\mathbf{S}}_{w1} + \hat{\mathbf{S}}_{w2}$) and the total ($\hat{\mathbf{S}} = \hat{\mathbf{S}}_{bb} + \hat{\mathbf{S}}_{ww}$) spin operators. Molar susceptibility χ_M was calculated by inserting these spin state energies into the Van Vleck equation [56] and was then fitted to the experimental susceptibility data by varying J_{bb} and J_{wb}. In all cases, the g-value was fixed to 2.00, as appropriate for high spin iron(III). This model could be successfully applied to the experimental data of **1–3** (Figure 2), confirming the starting assumptions.

Before discussing the best-fit results, we need to examine their reliability since the J_{bb} values obtained from the magnetic susceptibility data of butterfly-like $\{Fe_4(\mu_3\text{-}O)_2\}$ complexes can be largely under-determined [37,43]. This occurs because at low temperature, only $|5,5,S\rangle$ states are significantly populated, which differ in energy by

$$\Delta E(S', S) = -J_{wb}\ [S'(S' + 1) - S(S + 1)] \tag{3}$$

Thus, a change in J_{bb} does not affect the energy of the low-lying states and, hence, the magnetic susceptibility χ_M is scarcely sensitive to J_{bb} [35]. To analyze the confidence level of the best-fit parameters, we computed the sum of squared weighted residuals (*ssr*) for a region of the (J_{bb}, J_{wb}) plane about the best-fit values and found the constant-value contours of the difference $\Delta ssr = ssr - ssr_{min}$, i. e., the deviation from the minimum (best-fit) *ssr* (see Figure 2). The Δssr contours show a well-defined minimum in the (J_{bb}, J_{wb}) plane, proving that the best fit J_{bb} and J_{wb} values are reliable. Realistic estimates of the parameter errors could be obtained by projecting the appropriate constant Δssr contours on the J_{bb} and J_{wb} axes [58], and they are reported in Table 2. Both J_{bb} and J_{wb} were statistically significant for all the three complexes. The reason for this reliability lies in the peculiar spin level structure of **1–3** that we describe below.

Table 2. Best-fit parameters J_{bb} and J_{wb} (cm^{-1}), J_{bb}/J_{wb} ratio, and spin ground state for **1–3** obtained by fitting the butterfly model to the experimental $\chi_M T$ data.

	1 (NO$_2$)	**2 (Cl)** [1]	**3 (OMe)**
J_{bb} (cm^{-1})	−0.94 ± 0.06	−41.7 ± 0.2	−14.0 ± 0.3
J_{wb} (cm^{-1})	−1.20 ± 0.02	−25.2 ± 0.1	−8.2 ± 0.1
J_{bb}/J_{wb}	0.79 ± 0.05	1.66 ± 0.01	1.71 ± 0.04
Ground state	$|5,5,0\rangle$	$|3,5,2\rangle$	$|3,5,2\rangle$

[1] Model augmented with intermolecular exchange, $zj = -1.05 \pm 0.04$ cm^{-1} [59].

Both J_{wb} and J_{bb} of **1** are weaker than any tetranuclear iron butterfly complex collected in the literature [33], where J_{wb} ranges from −91.0 to −37.2 cm^{-1}, and J_{bb} ranges from −21.8 to −1.2 cm^{-1}. Furthermore, J_{wb} and J_{bb} show comparable strength (see Table 2). The J_{bb}/J_{wb} ratio of **1** is much larger than that of the reported butterfly {Fe$_4$(μ_3-O)$_2$} complexes (J_{bb}/J_{wb} ranging from 0.031 to 0.265) [33], with a single exception (J_{bb}/J_{wb} = 1.48) [35]. The ground state of **1** is the $|5,5,0\rangle$ singlet state, where the body–body antiferromagnetic interaction is completely frustrated [43]. The energy separation between spin states is small, and many of them are populated even at 5 K (see Figure S3 in Supplementary Materials), including states with S_{bb} < 5, because of the weakness of both coupling constants. Thus, χ_M significantly depends on J_{bb} through the energy difference between such states and the $|5,5,0\rangle$ ground state (cfr. Equation (3)). That is the reason why J_{bb} could be reliably determined from the susceptibility data of **1** [35].

The J_{bb} and J_{wb} of both **2** and **3** are in line with previously reported values [33] when separately considered, but the body–body exchange interaction is unusually strong compared to the wing–body interaction. Therefore, the body–body exchange interaction is not completely frustrated, resulting in the $|3,5,2\rangle$ ground state and the $|4,5,1\rangle$ and $|2,5,3\rangle$ lowest excited states. Thus, the spin states with unequal S_{bb} are populated even at low temperature, again ensuring a reliable determination of J_{bb}. The J_{bb}/J_{wb} ratio (*ca.* 1.7 for both **2** and **3**) is the highest obtained, and **2** and **3** are among the very few examples of compounds with a {Fe$_4$(μ_3-O)$_2$} core possessing a non-singlet ground state (quintet S = 2), in addition to the reported complex with J_{bb}/J_{wb} > 1 and S = 1 [35]. Different spin ground states can be instead stabilized for Mn$_4$O$_2$ clusters possessing a butterfly core structure [60,61].

It is not then apparent that a magneto–structural correlation [62] exists between the exchange coupling constants and spin state structure displayed by **1–3** and the structural features of their {Fe$_4$(μ_3-O)$_2$} cores. The pentacoordination of Fe$_w$ for sure introduces a novelty that affects the coupling constants J_{bb} and J_{wb} and the spin ground state, but this cannot be the discriminating factor, since all derivatives show this feature. The different orientation of the *tb* polyhedra with respect to the Fe$_4$O$_2$ plane between **1** on one side and **2** and **3** on the other side should not in principle affect the super-exchange magnetic communication path since it mainly depends on Fe–O distances and angles. The latter in any case show a certain non-negligible degree of variability among the three complexes, even if small, that alter the magnetic core. Furthermore, the presence of Cl···π interactions in **2** might further modulate its magnetic features.

2.4. Effect of the Substituents and QTAIM Analysis

The main differentiating element in **1–3** is for sure the substituent Z on the surrounding ligands, which displays a different electron demand, as shown by the Hammett-like σ_{ortho} constants [63,64]. Small, similar J constants are found when Z is strongly electron-withdrawing (NO$_2$, σ_{ortho} = +0.8), whereas moderately electron-withdrawing (Cl, σ_{ortho} = +0.2) and electron-donating (OMe, σ_{ortho} = −0.39) substituents are associated with more negative coupling constants and the peculiar J_{bb}/J_{wb} > 1. It is thus tempting to attribute (at least in part) the different magnetic properties of **1–3** to the different electronic availability in the {Fe$_4$(μ_3-O)$_2$} core, as we previously observed in electronically modulated Cu$_3$(μ_3-OH) trinuclear copper(II) complexes [8].

We have then performed a QTAIM topological analysis [65] of the computed electron density distribution (EDD) of **1–3**, aimed at determining a possible effect of the substituents Z on the EDD features of the metal core [66]. In Table 3 we report the integrated net charges of the iron ions and the μ_3-oxido anion. The computed charges on the Fe_b, Fe_w and μ_3-O atoms are not far from the corresponding values obtained from the QTAIM analysis of the experimental EDD for the carboxylate-bridge butterfly-like complex $[Fe^{III}_4(\mu_3\text{-O})_2(O_2CCMe_3)_8(NC_5H_4Me)_2]\cdot 2CH_3CN$ [34], amounting to 1.76, 1.67 and –0.91 e, respectively. While very small differences have been obtained along series **1–3**, a systematic lowering of the positive charge on Fe_b and a concomitant increase in absolute charge on Fe_w and μ_3-O can be detected, resulting in a progressive reduction of the $\{Fe_4(\mu_3\text{-O})_2\}$ positive charge going from the complex with the electron-withdrawing NO_2 group to the one bearing the electron-donating OMe group. This agrees with a modulating effect produced by Z on the EDD of the central core, which can consequently affect the magnetic properties in our Fe_4 clusters.

Table 3. Integrated net charge q (e) of the atomic basins Ω by the QTAIM partitioning in computed EDD of **1–3**.

	1 (NO$_2$)	2 (Cl)	3 (OMe)
Fe_b	1.899	1.898	1.897
Fe_w	1.836	1.838	1.839
μ_3-O	−1.204	−1.207	−1.208
$\Sigma\{Fe_4(\mu_3\text{-O})_2\}$	5.062	5.058	5.056

By looking at more detailed information as given by the values of the topological parameters at the Bond Critical Points (BCP) of the central core (see Table 4), we note a rather significant variation in the ρ_{BCP} values, and then in the bond strength, of the Fe–O bonds in the three compounds, thus emphasizing the less apparent trend as given by the bond lengths. The strength of the Fe_b–O bonds increases from **1** to **3**, while that of the Fe_w–O bonds decreases within the series, to a greater extent with respect to the Fe_b–O bonds. The ratio of the ρ_{BCP} values for the two types of bonds is in fact 0.706 for **1** and 0.742 for **3**. Owing to the large discrepancy between the experimental and theoretical ρ_{BCP} values obtained for the Fe–O bonds in the previously reported carboxylate-bridge butterfly-like complex [34], it is quite problematic to draw some conclusion on the different density values obtained for the Fe–O bonds in **1–3** with respect to other $\{Fe_4(\mu_3\text{-O})_2\}$ butterfly-like compounds. It is, however, interesting to note that the ρ_{BCP} ratios obtained for the two types of bonds in **1–3** are significantly larger than the corresponding value previously reported, 0.66 from both experiment and theory [34]. Finally, the character of the Fe–O bonds, as given by the Laplacian $\nabla^2\rho_{BCP}$ and the local energy densities G_{BCP}, V_{BCP} and $H_{BCP} = G_{BCP} + V_{BCP}$, is essentially unvaried along the series **1–3**, all quantities being indicative of a predominantly closed-shell character for these bonds ($\nabla^2\rho_{BCP} > 0$) with quite a small covalence degree, as given by negative but close to zero H_{BCP} values.

Table 4. Topological properties at selected BCPs of the central core in computed EDD of **1–3**.

	ρ_{BCP} (e Å^{-3})	$\nabla^2\rho_{BCP}$ (e Å^{-5})	G_{BCP} (Hartree Å^{-3})	V_{BCP} (Hartree Å^{-3})	H_{BCP} (Hartree Å^{-3})
Compound **1**					
Fe_b–O	0.628	11.7	0.132	−0.143	−0.011
Fe_w–O	0.889	16.9	0.210	−0.245	−0.035
Compound **2**					
Fe_b–O	0.636	11.9	0.134	−0.146	−0.012
Fe_w–O	0.870	16.6	0.205	−0.237	−0.032
Compound **3**					
Fe_b–O	0.640	12.0	0.135	−0.147	−0.012
Fe_w–O	0.863	16.5	0.202	−0.234	−0.032

3. Materials and Methods

3.1. General

All used chemicals were reagent grade, and solvents were used as received (Sigma Aldrich, Europe). Elemental analyses were performed at the Microanalytical Laboratory at the Università degli Studi di Milano. ESI-MS spectra were recorded on MeOH or MeCN solutions with a LCQ Advantage Thermofluxional instrument. Infrared spectra were recorded as KBr disks using a JASCO FT-IR 410 spectrophotometer with a 2 cm^{-1} resolution. Schiff bases H_2L^Z (Z = NO_2, Cl, OMe) were obtained following the synthetic method A reported in the literature [32].

3.2. Synthesis of [Fe$_4$(μ_3-O)$_2$(μ-L^{NO2})$_4$] (1)

First method: FeCl$_3$ (0.0651 g, 0.401 mmol) was added to a solution of H_2L^{NO2} (0.1511 g, 0.4025 mmol) in MeOH (6.0 mL) and NEt$_3$ (1.5 mL). The red mixture was left under stirring for 5 h, and then the red solid obtained was filtered, washed with MeOH, *i*Pr$_2$O and dried in vacuo (0.1364 g, 77.7%). *Second method:* FeCl$_3$ (0.0667 g, 0.411 mmol) was added to a solution of H_2L^{NO2} (0.1531 g, 0.4079 mmol) in MeCN (9.0 mL) and Et$_3$N (1.5 mL) and the red mixture was left under stirring for 5 h. The red solid obtained was filtered, and the reaction mixture was taken to dryness, yielding further solid. Both solids were extensively washed with a MeOH:H$_2$O 1:1 mixture and then dried in vacuo (0.1125 g, 63.09%). Anal. Calcd. for C$_{84}$H$_{60}$Fe$_4$N$_{12}$O$_{18}$ (1748.82): C, 57.69; H, 3.46; N, 9.61%. Found: C, 57.29; H, 3.65; N, 9.22%. MS (ESI): *m/z* 1771 ([M + Na]$^+$, 60%), 1748 ([M + H]$^+$, 100), 1302 ([Fe$_3$(O)(L^{NO2})$_3$]$^+$, 95). IR (KBr): 1611 ($\nu_{C=N}$), 1319 (ν_{NO2}) cm^{-1}. Crystals suitable for X-ray diffraction were obtained by diffusion of *i*Pr$_2$O into a MeOH solution of the title compound.

3.3. Synthesis of [Fe$_4$(μ_3-O)$_2$(μ-L^{Cl})$_4$] (2)

First method: The dark-red product was obtained as above in MeOH starting from FeCl$_3$ (0.0755 g, 0.465 mmol) and H_2L^{Cl} (0.1670 g, 0.4578 mmol) (0.1173 g, 60.06%). *Second method:* As above in MeCN from FeCl$_3$ (0.1595 g, 0.9833 mmol) and H_2L^{Cl} (0.3555 g, 0.9744 mmol) (0.1056 g, 25.40%). Anal. Calcd. for C$_{84}$H$_{60}$Cl$_4$Fe$_4$N$_8$O$_{10}$ (1706.64): C, 59.12; H, 3.54; N, 6.57%. Found: C, 59.24; H, 3.50; N, 6.18%. MS (ESI): *m/z* 1728 ([M + Na]$^+$, 30%), 1272 ([Fe$_3$(O)(L^{Cl})$_3$]$^+$, 100). IR (KBr): 1611 ($\nu_{C=N}$) cm^{-1}. Crystals suitable for X-ray diffraction were obtained by diffusion of *i*Pr$_2$O into a MeOH solution of the title compound.

3.4. Synthesis of [Fe$_4$(μ_3-O)$_2$(μ-L^{OMe})$_4$] (3)

First method: The dark-red solid was obtained as above in MeOH from FeCl$_3$ (0.1081 g, 0.6665 mmol) and H_2L^{OMe} (0.2388 g, 0.6626 mmol) (0.1944 g, 69.49%). *Second method:* As above in MeCN from FeCl$_3$ (0.1528 g, 0.9420 mmol) and H_2L^{OMe} (0.3359 g, 0.9320 mmol) (0.2489 g, 63.25%). Anal. Calcd. for C$_{88}$H$_{72}$Fe$_4$N$_8$O$_{14}$ (1688.97): C, 62.58; H, 4.30; N, 6.76%. Found: C, 62.85; H, 4.31; N, 6.24%. MS (ESI): *m/z* 1711 ([M + Na]$^+$, 10%), 1688 ([M + 1]$^+$, 15), 1258 ([Fe$_3$(O)(L^{OMe})$_3$]$^+$, 100). IR (KBr): 1613 ($\nu_{C=N}$) cm^{-1}.

3.5. Crystal Structure Determination

1·1.5*i*Pr$_2$O: C$_{186}$H$_{162}$Fe$_8$N$_{24}$O$_{39}$, *M* = 3804.20, monoclinic, *a* = 26.954(5), *b* = 26.974(5), *c* = 25.774(5) Å, *β* = 99.10(1)°, *V* = 18,503(16) Å^3, *T* = 293(2) K, space group *Cc* (no. 9), Z = 4, μ = (Mo-Kα) 0.690 mm^{-1}. A total of 17,490 reflections (9001 unique; R_{int} = 0.062) were collected at room temperature, employing a 0.28 × 0.12 × 0.10 mm crystal mounted on a Bruker APEX II CCD diffractometer using graphite-monochromatized Mo-Kα radiation (λ = 0.71073 Å). Final *R*1 [*wR*2] values were 0.0754 [0.2265] on *I* > 2σ(*I*) [all data].

2·2*i*Pr$_2$O: C$_{96}$H$_{88}$Cl$_4$Fe$_4$N$_8$O$_{12}$, *M* = 1910.94, tetragonal, *a* = 25.465(3), *c* = 14.683(2) Å, *V* = 9522(2) Å^3, *T* = 293(2) K, space group *P*–4 (no. 81), Z = 4, μ = (Mo-Kα) 0.772 mm^{-1}. A total of 55,409 reflections (17,810 unique; R_{int} = 0.060) were collected as before at room temperature, employing a 0.25 × 0.08 × 0.07 mm crystal. Final *R*1 [*wR*2] values were 0.0585 [0.1693] on *I* > 2σ(*I*) [all data].

Datasets were corrected for Lorentz-polarization effects and for absorption (*SAD-ABS* [67]). The structures were solved by direct methods (*SIR-97* [68]) and completed by iterative cycles of full-matrix least squares refinement on $F_o{}^2$ and ΔF synthesis using the *SHELXL-97* [69] program (*WinGX* suite) [70]. Hydrogen atoms, located on the ΔF maps, were allowed to ride on their carbon atoms. Crystallographic data for **1**·1.5*i*Pr$_2$O and **2**·2*i*Pr$_2$O (excluding structure factors) were deposited into the Cambridge Crystallographic Data Centre as supplementary publication no. 883278 and 883279, respectively. These data can be obtained free of charge via www.ccdc.cam.ac.uk/conts/retrieving.html (or from CCDC, 12 Union Road, Cambridge CB2 1EZ, UK; Fax: +44 1223 336033; e-mail: deposit@ccdc.cam.ac.uk).

3.6. Theoretical Calculations

Unrestricted DFT calculations were performed on **1–3** at the highest spin multiplicity 21 ($S = 10$), assuming all iron(III) ions in their high spin state ($S = 5/2$), using Gaussian 09 [71]. All the structures were optimized *in vacuo* with the 6-311G(d) basis set, starting from the X-ray geometries for **1** (molecule A) and **2**, and using **2** with the appropriated substitutions as a guess starting geometry for **3**. The functionals B3LYP [72,73] and M06 [74] were tested to check their performances in reproducing the X-ray structures of **1** and **2**. The latter functional, which was properly developed to treat organometallic complexes, provided the best agreement with the experimental geometries (see Tables S1 and S2 in Supplementary Materials for a full comparison between computed and experimental bond distances). Quantum Theory of Atoms In Molecules (QTAIM) [65], as implemented in AIMAll [75] was used for evaluating the net charges of the iron and oxido ions.

3.7. Magnetic Measurements

The magnetic moment μ of powder samples of **1–3** was measured between 5 and 300 K using a Quantum Design MPMS XL-5 SQUID magnetometer. Weighed amounts (about 15 mg) of **1–3** were sealed in polycarbonate capsules, and the magnetic moment μ was measured under an applied magnetic field of 1 kOe from 300 K down to 5 K. The molar susceptibility was obtained as $\chi_M = (\mu/H) \times (MW/m)$, where MW is the molecular weight of the complex, m is the sample mass, and H is the applied magnetic field. Diamagnetic contributions were subtracted from μ before calculating χ_M. The ligand diamagnetism was estimated using Pascal's constants [76].

4. Conclusions

The reaction of FeCl$_3$ with the Schiff bases H$_2$L^Z (Z = NO$_2$, Cl, OMe) led selectively to the tetranuclear iron compounds **1–3**, confirming the oligonucleation ability of these shortened ligands and the control of the nature of the oligonuclear compound upon substituent shift in *ortho* position of the central aryl ring. The analysis of the X-ray molecular structures of **1** and **2** and of the unrestricted-DFT computed geometries of all derivatives shows the similarity of the planar {Fe$_4$(μ_3-O)$_2$} cores, together with intramolecular Cl···π halogen bonds in **2**. In contrast, the J_{bb} and J_{wb} exchange coupling constants in **1–3** are different, and the unusually large J_{bb}/J_{wb} ratio for **2** and **3** suggests a quintet ($S = 2$) ground state for these compounds, which add up to another reported example of triplet ($S = 1$) ground state [35] being different from the singlet ground state ($S = 0$) usually reported for butterfly tetrairon(III) complexes [33].

The cores are slightly geometrically affected by the nature of the substituent Z, with the main differentiating factor given by the orientation of the *tb* polyhedra of the Fe$_w$ ions with respect to the Fe$_4$O$_2$ plane. The different spin ground states and the great variability of the J values can hardly be attributed to this structural difference. The unequal donating or accepting power of the substituent Z, which changes the EDD at the {Fe$_4$(μ_3-O)$_2$} core as confirmed by the topological QTAIM analysis, together with the different conformations of the surrounding ligands due to crystal packing and/or the steric and electronic effects of Z, may contribute to explaining the different magnetic properties of compounds **1–3**.

Further studies in this respect are certainly necessary and are planned in order to shed more light on our findings. In any case, the latter represents a solid starting point for investigating new butterfly Fe$_4$ clusters with different substituents on the surrounding Schiff bases to fully exploit the potentiality of these shortened salen-type ligand molecules as potent oligonucleating and magnetically modulating agents.

References

1. *Magnetism: Molecules to Materials*; Miller, J.S.; Drillon, M. (Eds.) Wiley-VCH: Weinheim, Germany; New York, NY, USA, 2001; ISBN 978-3-527-29772-6.
2. Gatteschi, D.; Sessoli, R.; Villain, J. *Molecular Nanomagnets*; Oxford University Press: Oxford, UK, 2006; ISBN 978-0-19-856753-0.
3. *Spin-Crossover Materials: Properties and Applications*; Halcrow, M.A. (Ed.) Wiley: Chichester, UK, 2013; ISBN 978-1-119-99867-9.
4. Miller, J.S. Organic- and Molecule-Based Magnets. *Mater. Today* **2014**, *17*, 224–235. [CrossRef]
5. Oshio, H.; Hoshino, N.; Ito, T.; Nakano, M. Single-Molecule Magnets of Ferrous Cubes: Structurally Controlled Magnetic Anisotropy. *J. Am. Chem. Soc.* **2004**, *126*, 8805–8812. [CrossRef] [PubMed]
6. Gregoli, L.; Danieli, C.; Barra, A.-L.; Neugebauer, P.; Pellegrino, G.; Poneti, G.; Sessoli, R.; Cornia, A. Magnetostructural Correlations in Tetrairon(III) Single-Molecule Magnets. *Chem. Eur. J.* **2009**, *15*, 6456–6467. [CrossRef] [PubMed]
7. Murali, M.; Nayak, S.; Costa, J.S.; Ribas, J.; Mutikainen, I.; Turpeinen, U.; Clémancey, M.; Garcia-Serres, R.; Latour, J.-M.; Gamez, P.; et al. Discrete Tetrairon(III) Cluster Exhibiting a Square-Planar Fe$_4$(μ_4-O) Core: Structural and Magnetic Properties. *Inorg. Chem.* **2010**, *49*, 2427–2434. [CrossRef] [PubMed]
8. Rigamonti, L.; Forni, A.; Sironi, M.; Ponti, A.; Ferretti, A.M.; Baschieri, C.; Pasini, A. Experimental and Theoretical Investigations on Magneto-Structural Correlation in Trinuclear Copper(II) Hydroxido Propellers. *Polyhedron* **2018**, *145*, 22–34. [CrossRef]
9. Winpenny, R.E.P. Serendipitous Assembly of Polynuclear Cage Compounds. *J. Chem. Soc. Dalton Trans.* **2002**, 1–10. [CrossRef]
10. Ohta, S.; Yokozawa, S.; Ohki, Y.; Tatsumi, K. Oxido-Bridged Di-, Tri-, and Tetra-Nuclear Iron Complexes Bearing Bis(Trimethylsilyl)Amide and Thiolate Ligands. *Inorg. Chem.* **2012**, *51*, 2645–2651. [CrossRef] [PubMed]
11. Botezat, O.; van Leusen, J.; Kögerler, P.; Baca, S.G. Tuning the Condensation Degree of {Fe$^{III}_n$} Oxo Clusters via Ligand Metathesis, Temperature, and Solvents. *Inorg. Chem.* **2018**, *57*, 7904–7913. [CrossRef] [PubMed]
12. Hale, A.R.; Lott, M.E.; Peralta, J.E.; Foguet-Albiol, D.; Abboud, K.A.; Christou, G. Magnetic Properties of High-Nuclearity Fe$_x$-Oxo(x = 7, 22, 24) Clusters Analyzed by a Multipronged Experimental, Computational, and Magnetostructural Correlation Approach. *Inorg. Chem.* **2022**, *61*, 11261–11276. [CrossRef] [PubMed]
13. Nachtigall, O.; Kusserow, M.; Clérac, R.; Wernsdorfer, W.; Menzel, M.; Renz, F.; Mrozinski, J.; Spandl, J. [Fe$_{19}$] "Super-Lindqvist" Aggregate and Large 3D Interpenetrating Coordination Polymer from Solvothermal Reactions of [Fe$_2$(OtBu)$_6$] with Ethanol. *Angew. Chem. Int. Ed.* **2015**, *54*, 10361–10364. [CrossRef] [PubMed]
14. Cozzi, P.G. Metal–Salen Schiff Base Complexes in Catalysis: Practical Aspects. *Chem. Soc. Rev.* **2004**, *33*, 410–421. [CrossRef] [PubMed]

15. Rigamonti, L.; Demartin, F.; Forni, A.; Righetto, S.; Pasini, A. Copper(II) Complexes of Salen Analogues with Two Differently Substituted (Push−Pull) Salicylaldehyde Moieties. A Study on the Modulation of Electronic Asymmetry and Nonlinear Optical Properties. *Inorg. Chem.* **2006**, *45*, 10976–10989. [CrossRef] [PubMed]

16. Rigamonti, L.; Forni, A.; Righetto, S.; Pasini, A. Push-Pull Unsymmetrical Substitution in Nickel(II) Complexes with Tetradentate N_2O_2 Schiff Base Ligands: Synthesis, Structures and Linear-Nonlinear Optical Studies. *Dalton Trans.* **2019**, *48*, 11217–11234. [CrossRef] [PubMed]

17. Rigamonti, L.; Forni, A.; Cariati, E.; Malavasi, G.; Pasini, A. Solid-State Nonlinear Optical Properties of Mononuclear Copper(II) Complexes with Chiral Tridentate and Tetradentate Schiff Base Ligands. *Materials* **2019**, *12*, 3595. [CrossRef] [PubMed]

18. Downing, R.S.; Urbach, F.L. Circular Dichroism of Square-Planar, Tetradentate Schiff Base Chelates of Copper(II). *J. Am. Chem. Soc.* **1969**, *91*, 5977–5983. [CrossRef]

19. Kleij, A.W. Nonsymmetrical Salen Ligands and Their Complexes: Synthesis and Applications. *Eur. J. Inorg. Chem.* **2009**, *2009*, 193–205. [CrossRef]

20. Mazzoni, R.; Roncaglia, F.; Rigamonti, L. When the Metal Makes the Difference: Template Syntheses of Tridentate and Tetradentate Salen-Type Schiff Base Ligands and Related Complexes. *Crystals* **2021**, *11*, 483. [CrossRef]

21. Ashoka Sahadevan, S.; Cadoni, E.; Monni, N.; Sáenz de Pipaón, C.; Galan Mascaros, J.-R.; Abhervé, A.; Avarvari, N.; Marchiò, L.; Arca, M.; Mercuri, M.L. Structural Diversity in a New Series of Halogenated Quinolyl Salicylaldimides-Based Fe^{III} Complexes Showing Solid-State Halogen-Bonding/Halogen⋯Halogen Interactions. *Cryst. Growth Des.* **2018**, *18*, 4187–4199. [CrossRef]

22. Chowdhury, T.; Adhikary, A.; Roy, M.; Zangrando, E.; Samanta, D.; Das, D. Mapping of Solvent-Mediated Molecular Self-Assembly of Iron(III) Discrete Compounds: Exploring Their Magnetic Behavior and Phosphatase-Like Activity. *Cryst. Growth Des.* **2020**, *20*, 1254–1265. [CrossRef]

23. Fik, M.A.; Czepa, W.; Kubicki, M.; Patroniak, V. Formation of Non-Covalent Porous Framework with Fe Ions and N_2O Schiff Base Ligand: Structural and Thermal Studies. *Supramol. Chem.* **2017**, *29*, 643–650. [CrossRef]

24. Pasini, A.; Demartin, F.; Piovesana, O.; Chiari, B.; Cinti, A.; Crispu, O. Novel Copper(II) Complexes of "Short" Salen Homologues. Structure and Magnetic Properties of the Tetranuclear Complex [$Cu_2(L^2)_2$]$_2$ [H_2L^2 = Phenyl-*N*,*N* ′-Bis(Salicylidene)Methanediamine]. *J. Chem. Soc. Dalton Trans.* **2000**, *19*, 3467–3472. [CrossRef]

25. Chiari, B.; Cinti, A.; Crispu, O.; Demartin, F.; Pasini, A.; Piovesana, O. Binuclear Co(II)Co(II), Co(II)Co(III) and Co(III)Co(III) Complexes of "Short" Salen Homologues Derived from the Condensation of Salicylaldehyde and Methanediamine or Phenyl-methanediamines. Synthesis, Structures and Magnetism. *J. Chem. Soc. Dalton Trans.* **2001**, *24*, 3611–3616. [CrossRef]

26. Chiari, B.; Cinti, A.; Crispu, O.; Demartin, F.; Pasini, A.; Piovesana, O. New Pentanuclear Mixed Valence Co(II)–Co(III) Complexes of "Short" Salen Homologues. *J. Chem. Soc. Dalton Trans.* **2002**, 4672–4677. [CrossRef]

27. Rigamonti, L.; Zardi, P.; Carlino, S.; Demartin, F.; Castellano, C.; Pigani, L.; Ponti, A.; Ferretti, A.M.; Pasini, A. Selective Formation, Reactivity, Redox and Magnetic Properties of Mn^{III} and Fe^{III} Dinuclear Complexes with Shortened Salen-Type Schiff Base Ligands. *Int. J. Mol. Sci.* **2020**, *21*, 7882. [CrossRef] [PubMed]

28. Rigamonti, L.; Forni, A. Effect of Crystal Packing and Coordinated Solvent Molecules on Metal-Ligand Bond Distances in Linear Trinuclear Nickel Compounds with Bridging Acetato and Schiff Base Ligands. *Inorg. Chim. Acta* **2018**, *473*, 216–222. [CrossRef]

29. Rigamonti, L.; Forni, A.; Pievo, R.; Reedijk, J.; Pasini, A. Copper(II) Compounds with NNO Tridentate Schiff Base Ligands: Effect of Subtle Variations in Ligands on Complex Formation, Structures and Magnetic Properties. *Inorg. Chim. Acta* **2012**, *387*, 373–382. [CrossRef]

30. Rigamonti, L.; Forni, A.; Pievo, R.; Reedijk, J.; Pasini, A. Synthesis, Crystal Structures and Magnetic Properties of Dinuclear Copper(II) Compounds with NNO Tridentate Schiff Base Ligands and Bridging Aliphatic Diamine and Aromatic Diimine Linkers. *Dalton Trans.* **2011**, *40*, 3381–3393. [CrossRef] [PubMed]

31. Rigamonti, L.; Cinti, A.; Forni, A.; Pasini, A.; Piovesana, O. Copper(II) Complexes of Tridentate Schiff Bases of 5-Substituted Salicylaldehydes and Diamines—The Role of the Substituent and the Diamine in the Formation of Mono-, Di- and Trinuclear Species—Crystal Structures and Magnetic Properties. *Eur. J. Inorg. Chem.* **2008**, *2008*, 3633–3647. [CrossRef]

32. Takajo, T.; Kambe, S.; Ando, W. Synthesis of *N*,*N*′-Bis[2-Hydroxybenzylidene]Arylmethanediamines. *Synthesis* **1984**, *1984*, 256–259. [CrossRef]

33. Baca, S.G.; Filippova, I.G.; Keene, T.D.; Botezat, O.; Malaestean, I.L.; Stoeckli-Evans, H.; Kravtsov, V.C.; Chumacov, I.; Liu, S.; Decurtins, S. Iron(III)-Pivalate-Based Complexes with Tetranuclear {$Fe_4(\mu_3$-O)$_2$}$^{8+}$ Cores and *N*-Donor Ligands: Formation of Cluster and Polymeric Architectures. *Eur. J. Inorg. Chem.* **2011**, *2011*, 356–367. [CrossRef]

34. Overgaard, J.; Hibbs, D.E.; Rentschler, E.; Timco, G.A.; Larsen, F.K. Experimental and Theoretical Electron Density Distribution and Magnetic Properties of the Butterfly-like Complex [$Fe_4O_2(O_2CCMe_3)_8(NC_5H_4Me)_2$]·$2CH_3CN$. *Inorg. Chem.* **2003**, *42*, 7593–7601. [CrossRef] [PubMed]

35. Stamatatos, T.C.; Boudalis, A.K.; Sanakis, Y.; Raptopoulou, C.P. Reactivity and Structural and Physical Studies of Tetranuclear Iron(III) Clusters Containing the [$Fe_4(\mu_3$-O)$_2$]$^{8+}$ "Butterfly" Core: An Fe^{III}$_4$ Cluster with an *S* = 1 Ground State. *Inorg. Chem.* **2006**, *45*, 7372–7381. [CrossRef] [PubMed]

36. Gorun, S.M.; Lippard, S.J. Synthesis, Structure, and Characterization of the Tetranuclear Iron(III) Oxo Complex [$Fe_4O_2(BICOH)_2(BICO)_2$ $(O_2CPh)_4$]Cl_2. *Inorg. Chem.* **1988**, *27*, 149–156. [CrossRef]

37. Pichon, C.; Dolbecq, A.; Mialane, P.; Marrot, J.; Rivière, E.; Goral, M.; Zynek, M.; McCormac, T.; Borshch, S.A.; Zueva, E.; et al. Fe$_2$ and Fe$_4$ Clusters Encapsulated in Vacant Polyoxotungstates: Hydrothermal Synthesis, Magnetic and Electrochemical Properties, and DFT Calculations. *Chem. Eur. J.* **2008**, *14*, 3189–3199. [CrossRef] [PubMed]

38. Wu, L.; Pressprich, M.; Coppens, P.; DeMarco, M.J. A New Tetranuclear Iron(III) Complex with an [Fe$_4$O$_2$] Core: Synthesis, Structure and Mössbauer Studies of [Fe$_4$(μ_3-O)$_2$(μ-O$_2$CCH$_3$)$_6$Cl$_2$(3-Mepy)$_4$].CH$_3$CN (3-Mepy = 3-Methylpyridine). *Acta Crystallogr. C Cryst. Struct. Commun.* **1993**, *49*, 1255–1258. [CrossRef]

39. Bacsa, J.; Zhao, H.; Dunbar, K.R. Two New Soluble Iron–Oxo Complexes: [Fe$_2$(μ-O)(μ-O$_2$CCF$_3$)$_2$(O$_2$CCF$_3$)$_2$(C$_{10}$H$_8$N$_2$)$_2$] and [Fe$_4$(μ_3-O)$_2$(μ-O$_2$CCF$_3$)$_6$(O$_2$CCF$_3$)$_2$(C$_{10}$H$_8$N$_2$)$_2$]·CF$_3$CO$_2$H. *Acta Crystallogr. C Cryst. Struct. Commun.* **2003**, *59*, m561–m564. [CrossRef] [PubMed]

40. Cortés, P.; Atria, A.M.; Garland, M.T.; Baggio, R. Two Oxo Complexes with Tetranuclear [Fe$_4$(μ_3-O)$_2$]$^{8+}$ and Trinuclear [Fe$_3$(μ_3-O)]$^{7+}$ Units. *Acta Crystallogr. C Cryst. Struct. Commun.* **2006**, *62*, m297–m302. [CrossRef] [PubMed]

41. Mulyana, Y.; Nafady, A.; Mukherjee, A.; Bircher, R.; Moubaraki, B.; Murray, K.S.; Bond, A.M.; Abrahams, B.F.; Boskovic, C. New Family of Ferric Spin Clusters Incorporating Redox-Active *Ortho*-Dioxolene Ligands. *Inorg. Chem.* **2009**, *48*, 7765–7781. [CrossRef] [PubMed]

42. Armstrong, W.H.; Roth, M.E.; Lippard, S.J. Tetranuclear Iron-Oxo Complexes. Synthesis, Structure, and Properties of Species Containing the Nonplanar {Fe$_4$O$_2$}$^{8+}$ Core and Seven Bridging Carboxylate Ligands. *J. Am. Chem. Soc.* **1987**, *109*, 6318–6326. [CrossRef]

43. McCusker, J.K.; Vincent, J.B.; Schmitt, E.A.; Mino, M.L.; Shin, K.; Coggin, D.K.; Hagen, P.M.; Huffman, J.C.; Christou, G.; Hendrickson, D.N. Molecular Spin Frustration in the [Fe$_4$O$_2$]$^{8+}$ Core: Synthesis, Structure, and Magnetochemistry of Tetranuclear Iron-Oxo Complex [Fe$_4$O$_2$(O$_2$CR)$_7$(Bpy)$_2$](ClO$_4$) (R = Me, Ph). *J. Am. Chem. Soc.* **1991**, *113*, 3012–3021. [CrossRef]

44. Wemple, M.W.; Coggin, D.K.; Vincent, J.B.; McCusker, J.K.; Streib, W.E.; Huffman, J.C.; Hendrickson, D.N.; Christou, G. New Tetranuclear Metal Carboxylate Clusters with the [M$_4$(μ_3-O)$_2$]$^{8+}$ (M = Mn^{III} or Fe^{III}) Cores: Crystal Structures and Properties of [Mn$_4$O$_2$Cl$_2$(O$_2$CC$_6$H$_3$F$_2$-3,5)$_6$(Py)$_4$], [Fe$_4$O$_2$Cl$_2$(O$_2$CMe)$_6$(Bpy)$_2$] and [NBun$_4$][Fe$_4$O$_2$(O$_2$CMe)$_7$(Pic)$_2$]. *J. Chem. Soc., Dalton Trans.* **1998**, *4*, 719–726. [CrossRef]

45. Gkioni, C.; Boudalis, A.K.; Sanakis, Y.; Psycharis, V.; Raptopoulou, C.P. 2-Pyridyl Ketone Oximes in Iron(III) Carboxylate Chemistry: Synthesis, Structural and Physical Studies of Tetranuclear Clusters Containing the [Fe$_4$(μ_3-O)$_2$]$^{8+}$ 'Butterfly' Core. *Polyhedron* **2009**, *28*, 3221–3226. [CrossRef]

46. Dutta, A.K.; Maji, S.K.; Dutta, S.; Robert Lucas, C.; Adhikary, B. Synthesis, Structural and Magnetic Properties of Oxo-, Chloroacetato-Bridged Tetra-Nuclear Iron(III) Complex. *J. Mol. Struct.* **2012**, *1029*, 68–74. [CrossRef]

47. Dutta, A.K.; Maji, S.K.; Dutta, S.; Robert Lucas, C.; Adhikary, B. Syntheses, Crystal Structure, Spectroscopic, Redox and Magnetic Properties of Oxo- and Carboxylato-Bridged Polynuclear Iron(III) Complexes with Phenolate- and Pyridine-Substituted Benzimidazole Ligands. *Polyhedron* **2012**, *44*, 34–43. [CrossRef]

48. Luo, Y.-H.; Chen, C.; Li, Y.-J.; Wang, J.-W.; Sun, B.-W. Protonation-Induced Color Change of an Amino Group Functionalized [Fe4(M3-O)2]8+ Cluster. *Dyes Pigment.* **2017**, *143*, 239–244. [CrossRef]

49. Pal, C.K.; Mahato, S.; Yadav, H.R.; Shit, M.; Choudhury, A.R.; Biswas, B. Bio-Mimetic of Catecholase and Phosphatase Activity by a Tetra-Iron(III) Cluster. *Polyhedron* **2019**, *174*, 114156. [CrossRef]

50. Lutsenko, I.A.; Kiskin, M.A.; Baravikov, D.E.; Nelyubina, Y.V.; Primakov, P.V.; Eremenko, I.L. Chemical Design of Heterometallic Carboxylate Structures with Fe^{3+} and Ag$^+$ Ions as a Rational Synthetic Approach. *Mendeleev Commun.* **2021**, *31*, 628–630. [CrossRef]

51. Dimiza, F.; Hatzidimitriou, A.G.; Sanakis, Y.; Papadopoulos, A.N.; Psomas, G. Trinuclear and Tetranuclear Iron(III) Complexes with Fenamates: Structure and Biological Profile. *J. Inorg. Biochem.* **2021**, *218*, 111410. [CrossRef] [PubMed]

52. *Halogen Bonding: Fundamentals and Applications*; Metrangolo, P.; Resnati, G.; Arman, H.D. (Eds.) Structure and Bonding; Springer: Berlin, Germany, 2008; ISBN 978-3-540-74329-3.

53. Forni, A.; Pieraccini, S.; Rendine, S.; Gabas, F.; Sironi, M. Halogen-Bonding Interactions with π Systems: CCSD(T), MP2, and DFT Calculations. *ChemPhysChem* **2012**, *13*, 4224–4234. [CrossRef] [PubMed]

54. Forni, A.; Pieraccini, S.; Rendine, S.; Sironi, M. Halogen Bonds with Benzene: An Assessment of DFT Functionals. *J. Comput. Chem.* **2014**, *35*, 386–394. [CrossRef] [PubMed]

55. Forni, A.; Pieraccini, S.; Franchini, D.; Sironi, M. Assessment of DFT Functionals for QTAIM Topological Analysis of Halogen Bonds with Benzene. *J. Phys. Chem. A* **2016**, *120*, 9071–9080. [CrossRef]

56. Kahn, O. *Molecular Magnetism*; Wiley-VCH: Weinheim, Germany, 1993.

57. Kambe, K. On the Paramagnetic Susceptibilities of Some Polynuclear Complex Salts. *J. Phys. Soc. Jpn.* **1950**, *5*, 48–51. [CrossRef]

58. Press, W.H.; Teukolsky, S.A.; Vetterling, W.T.; Flannery, B.P. *Numerical Recipes in C: The Art of Scientific Computing*, 2nd ed.; Cambridge University Press: Cambridge, UK; New York, NY, USA, 1992; ISBN 978-0-521-43108-8.

59. O'Connor, C.J. Magnetochemistry-Advances in Theory and Experimentation. In *Progress in Inorganic Chemistry*; Lippard, S.J., Ed.; John Wiley & Sons, Inc.: Hoboken, NJ, USA, 2007; pp. 203–283; ISBN 978-0-470-16630-7.

60. Chaudhuri, P.; Rentschler, E.; Birkelbach, F.; Krebs, C.; Bill, E.; Weyhermüller, T.; Flörke, U. Ground Spin State Variation in Carboxylate-Bridged Tetranuclear [Fe$_2$Mn$_2$O$_2$]$^{8+}$ Cores and a Comparison with Their [Fe$_4$O$_2$]$^{8+}$ and [Mn$_4$O$_2$]$^{8+}$ Congeners. *Eur. J. Inorg. Chem.* **2003**, *2003*, 541–555. [CrossRef]

61. Jerzykiewicz, L.B.; Utko, J.; Duczmal, M.; Starynowicz, P.; Sobota, P. Tetranuclear Manganese Complexes with [Mn$^{II}_4$] and [Mn$^{II}_2$Mn$^{III}_2$] Units: Syntheses, Structures, Magnetic Properties, and DFT Study. *Eur. J. Inorg. Chem.* **2010**, *2010*, 4492–4498. [CrossRef]

62. Mitchell, K.J.; Abboud, K.A.; Christou, G. Magnetostructural Correlation for High-Nuclearity Iron(III)/Oxo Complexes and Application to Fe$_5$, Fe$_6$, and Fe$_8$ Clusters. *Inorg. Chem.* **2016**, *55*, 6597–6608. [CrossRef]

63. Carey, F.A.; Sundberg, R.J. *Advanced Organic Chemistry*, 5th ed.; Springer: New York, NY, USA, 2007; ISBN 978-0-387-44897-8.

64. Takahata, Y.; Chong, D.P. Estimation of Hammett Sigma Constants of Substituted Benzenes through Accurate Density-Functional Calculation of Core-Electron Binding Energy Shifts. *Int. J. Quantum Chem.* **2005**, *103*, 509–515. [CrossRef]

65. Bader, R.F.W. *Atoms in Molecules: A Quantum Theory*; The International Series of Monographs on Chemistry; Oxford University Press: Oxford, UK; New York, NY, USA, 1994; ISBN 978-0-19-855865-1.

66. Rigamonti, L.; Rusconi, M.; Forni, A.; Pasini, A. The Role of the Atomic Charges on the Ligands and Platinum(II) in Affecting the Cis and Trans Influences in [PtXL(PPh$_3$)$_2$]$^+$ Complexes (X = NO$_3$, Cl, Br, I; L = 4-Substituted Pyridines, Amines, PPh$_3$). A ^{31}P NMR and DFT Investigation. *Dalton Trans.* **2011**, *40*, 10162. [CrossRef]

67. Sheldrick, G.M. *SADABS-2008/1—Bruker AXS Area Detector Scaling and Absorption Correction*; Bruker AXS: Madison, WI, USA, 2008.

68. Altomare, A.; Burla, M.C.; Camalli, M.; Cascarano, G.L.; Giacovazzo, C.; Guagliardi, A.; Moliterni, A.G.G.; Polidori, G.; Spagna, R. *SIR* 97: A New Tool for Crystal Structure Determination and Refinement. *J. Appl. Crystallogr.* **1999**, *32*, 115–119. [CrossRef]

69. Sheldrick, G.M. Crystal Structure Refinement with *SHELXL. Acta Crystallogr. Sect. C* **2015**, *71*, 3–8. [CrossRef] [PubMed]

70. Farrugia, L.J. *WinGX* and *ORTEP for Windows*: An Update. *J. Appl. Crystallogr.* **2012**, *45*, 849–854. [CrossRef]

71. Frisch, M.J.; Trucks, G.W.; Schlegel, H.B.; Scuseria, G.E.; Robb, M.A.; Cheeseman, J.R.; Scalmani, G.; Barone, V.; Petersson, G.A.; Nakatsuji, H.; et al. *Gaussian 09, Revision A.02*; Gaussian, Inc.: Wallingford, CT, USA, 2009.

72. Lee, C.; Yang, W.; Parr, R.G. Development of the Colle-Salvetti Correlation-Energy Formula into a Functional of the Electron Density. *Phys. Rev. B* **1988**, *37*, 785–789. [CrossRef] [PubMed]

73. Vosko, S.H.; Wilk, L.; Nusair, M. Accurate Spin-Dependent Electron Liquid Correlation Energies for Local Spin Density Calculations: A Critical Analysis. *Can. J. Phys.* **1980**, *58*, 1200–1211. [CrossRef]

74. Zhao, Y.; Truhlar, D.G. The M06 Suite of Density Functionals for Main Group Thermochemistry, Thermochemical Kinetics, Noncovalent Interactions, Excited States, and Transition Elements: Two New Functionals and Systematic Testing of Four M06-Class Functionals and 12 Other Functionals. *Theor. Chem. Acc.* **2008**, *120*, 215–241. [CrossRef]

75. Todd, K.A. *AIMAll (Version 12.05.09)*; TK Gristmill Software: Overland Park KS, USA, 2012.

76. Bain, G.A.; Berry, J.F. Diamagnetic Corrections and Pascal's Constants. *J. Chem. Educ.* **2008**, *85*, 532–536. [CrossRef]